ANNALES
UNIVERSITATIS MARIAE CURIE-SKŁODOWSKA
LUBLIN – POLONIA

VOL. LX, 7 SECTIO AA 2005

Development and validation of a methodology for the reliable characterization of porous materials

L. F. Vega[1*], C. Herdes[1] and M. A. Santos[2]
[1]*Institut de Ciència de Materials de Barcelona, (ICMAB-CSIC), Consejo Superior de Investigaciones Científicas, Campus de la U.A.B., Bellaterra, 08193 Barcelona, Spain*
[2]*Center for Computational Biology. The Hospital for Sick Children. Toronto, Ontario, Canada M5G 1X8*

This article summarizes the application of a methodology for Pore Size Distribution (PSD) calculations in which a regularization procedure is combined with individual adsorption isotherms obtained from Grand Canonical Monte Carlo simulations. The methodology combines mathematical and physical requirements in order to obtain reliable PSDs. A protocol is proposed to isolate the different effects contributing to the obtained PSD function, in a systematic manner. The PSD robustness is measured imposing random errors over the experimental data. The methodology is first applied to a member of the MCM-41, chosen for its particular structure, in which the adsorption takes place in non-interconnected pores. The accuracy of the results shows the precision of the method for this case, validating the independent pore model. The method is next applied to a SBA-15 material, as representative of materials with both, meso- and micropores, checking the reliability of the method for materials with connected pores. Excellent agreement is also found in this case. In addition, molecular simulations provide new insights into the studied systems, pointing out the need of high-resolution isotherms to describe the presence of complementary microporosity in the SBA material.

* Corresponding author: lvega@icmab.es

1. INTRODUCTION

Adsorbent and catalytic materials are used for several industrial applications, ranging from chemical to pharmaceutical, among others. In order to optimize their performance a precise characterization of the materials is needed prior they are put into final use. Several characterization techniques are used for this purpose. Among them, the structural characterization of porous materials is routinely obtained by adsorption studies, where the adsorption isotherm curves need to be interpreted through a model. Surface areas and Pore Size Distributions (PSD) are obtained by this procedure.

Due to its scientific and technical relevance, the development of consistent methods for the interpretation of adsorption isotherms has been the subject of several research efforts for almost 60 years. The most extended methods developed from the classical approach are those of Brunauer, Emmet and Teller (BET), the Gibbs-Kelvin method (GK), the Dubinin and Radushkevich (DR) equation, and their modifications, based on phenomenological assumptions with well-known limitations. For instance, the GK method assumes subcritical adsorbate homogeneity and incompressibility, gas phase ideality and independency of the interfacial tension of the liquid of its curvature; the BET model was derived assuming identity to bulk liquid of all adsorbed layers beyond the first and absence of lateral interactions in adsorbed layers; the DR method assumes volume filling of pores and Gaussian distribution of micropores, etc. Although their limitations are well-known, some of these methods are still in use for the characterization of adsorbent materials. For a detailed discussion on the subject the reader is referred to [1]. In fact, the development of reliable methods for the accurate characterization of porous materials remains an on-top and motivating problem now-a-days [1], especially for materials with a wide range of pore sizes and shapes, and for heterogeneous surface materials. Research is focused on two main topics, both related to obtain the PSD from inversion of the adsorption integral equation: a reliable method to obtain the kernel of individual adsorption isotherms, and a robust mathematical procedure to invert the integral.

Statistical mechanics provides two approaches to obtain the individual adsorption isotherms: the density functional theory (DFT) and molecular simulations (MS). Different versions of DFT have been used to characterize materials, most of them focused on carbons [2-7]. Other materials also characterized by DFT include controlled pore glasses [8,9], MCM-41 and MCM-48 [10-12], and other hexagonal mesoporous materials [13]. A main limitation of DFT in this context is that it is difficult to discern the uncertainties coming from the approximations made in the theory to those coming from the inversion of the integral and/or the model used. Also, the extension of the theory to non-spherical fluids, polar fluids and non-homogeneous surfaces is not

straightforward. An alternative to DFT is the use of molecular simulations (MS). Although more expensive from the computational point of view, MS offers several advantages over the DFT approach: 1) the statistical mechanical equations are solved exactly for the prescribed model of the pore geometry and intermolecular interactions, 2) its versatility permits the incorporation of surface structure and heterogeneity, a variety of pore geometries and irregularities and 3) it is straightforward to implement for different adsorbates, including chain and associating molecules. At present, the high speed of computers makes simulations a feasible tool for the generation of the individual adsorption isotherms. The most appropriate MS technique applied to adsorption in porous materials is the Grand Canonical Monte Carlo simulation method (GCMC) [14]. Several authors have used GCMC for the characterization of porous materials, mainly focused on carbons [15-21].

Progress in molecular modelling of adsorption phenomena by means DFT calculations and MS has led to a better understanding of the specific interactions of the adsorbed species with the porous material [2-13,15-25]. However, in some of these works some limitations of the methodology for the determination of the PSD could have been screened either by intrinsic drawbacks in the material selection such as high tortousity, effective surface area far away from individual pore model applicable conditions (e.g. activated carbon, controlled pore glasses, and some others), by approximations made in the applied theories, and/or by ignoring relevant energetic heterogeneities. A way to isolate the impact of each assumption is by first applying the methodology to materials with well defined geometry and morphology. In this case, deviations would come either from the method used to model the individual adsorption isotherms (DFT or MS), which can be refined by direct comparison with the experimental data, or by ignoring the connection among the pores. If the methodology is applied to porous materials with well defined geometry and unconnected pores, the only assumption to be validated is the adsorption behaviour in individual pores, in addition to the mathematical procedure to invert the adsorption integral [26].

In fact, the mathematical procedure used to invert the adsorption integral is a key issue in obtaining reliable PSD's. The robust procedure to invert the integral turns out to be at least as important as the physical considerations we have mentioned above. The problem arises from the nature of the equation from which the PSD function is inferred, since solving this integral equation is an "ill-posed" problem, i.e., there are several PSD functions compatible with the experimental adsorption isotherm. The inversion of the integral can be performed by proposing an analytical function, as a reasonable representation of the PSD, or by direct numerical inversion. The analytical functions are usually based on physical arguments and their parameters are fitted to the adsorption data. However, as Davies et al. [21] pointed out, there is a danger in constraining the

PSD to conform to the particular functional form adopted. The danger is that we are not longer determining whether any PSD can be fitted to the data, but rather whether a PSD conforming to the proposed functional form exists. In contrast, the numerical inversion of the integral shows the advantage of being more flexible, since the PSD is not constrained a priori to any functional form. An elegant and powerful way to solve this integral equation is by using regularization methods (see, for instance, references [8,13,16]). These methods also need of additional information on the system, which is used to select one of the PSD's among all possible satisfying the inversion equation from the knowledge of the experimental adsorption isotherms and some additional requirements, as stated in this article.

The work presented here is part of an on-going project on developing reliable molecular simulation-based tools for the optimal design and characterization of meso- and microporous materials for specific applications [8,26-29]. The final goal is to propose a methodology for the systematic characterization of different types of materials in a predictive manner, taking advantage of the molecular information of the system. Within this framework, we have developed a protocol to obtain robust PSD of adsorbent materials by combining GCMC simulations with a regularization procedure and experimental data. As a first step in checking the reliability of the procedure for the characterization of porous materials, the method is applied to selected MCM-41 materials, chosen for their well defined pore geometry (cylindrical) and unconnected pores. The methodology is next applied to an SBA-15 material. This material is also an excellent candidate to check the developed methodology for PSD analysis: it is made up of well-defined cylindrical mesopores with a narrow PSD, measurable from other experimental techniques; it also presents a microporous region which can be explored with this type of theoretical methods. In SBA-15 materials, the pores have a defined geometry, but they are connected.

An additional reason to choose these particular materials for validating the methodology is their great interest for several industrial applications. In fact, it was the demand from the industrial sector of large pore-size adsorbents with well-defined geometry who endorsed the inception of the family of mesoporous molecular sieves M41S. One of the highlighted members is the hexagonally ordered MCM-41, coined by Mobil Corporation in the early 90's [30]. MCM-41 was manufactured under conditions where silica-surfactant self-assembly occurred simultaneously with condensation of the inorganic species, yielding mesoscopically ordered composites. The research evolution was driven to the extension of surfactant-template procedures, in order to include a wide range of compositions and to explore different structure-directing functions, establishing the aim of several theoretical and experimental studies [31-37]. For this purpose, nonionic block copolymers, an interesting class of structure-directing agents

whose self-assembly characteristics lead to kinetically quenched structures, were used on those synthesis. Block copolymers have the advantage over surfactants that their ordering properties can be nearly continuously tuned by adjusting solvent composition, molecular weight, or copolymer architecture. The next generation of hexagonal mesoporous materials such as SBA-15 (Santa Barbara-x) [38] and PHTS (Plugged hexagonal templated silica) [39] have attracted much interest on both science and technology fields, due to their potential applications in shape-selective catalysis, separation of large molecules, purification of fluids, fabrication of membranes and also as directing patterns for other materials. SBA-15 high ordered mesoporous silica exhibits a remarkable hydrothermal stability [40] compared to MCM-41, and can be synthesized in a wide range of pore sizes and particle morphologies. SBA-15 has already been tested for several applications in the fields of catalysis, separations, and advanced optical materials [40-46]. Most of their key properties have been attributed to the particular arrangement of pores in these materials: they consist of mesoporous cylinders connected by nano- and microporous inside the walls [39].

The particular structure of MCM-41 makes possible a reliable structural characterization from adsorption data. The characterization by adsorption can be validated with some alternative experimental techniques, including XRD. Neimark et al. [11], had conducted a pore size analysis of MCM-41 by means of nitrogen and argon adsorption/desorption data. The study was performed in the following five steps: 1) they synthesized references samples with uniform cylindrical pore channels of different sizes, 2) they characterized their structures using X-ray diffraction (XRD) and adsorption of nitrogen at 77 K and argon at 77 and 87 K, 3) they determined and verified the intermolecular interaction parameters for non-local density functional theory (NLDFT) model of nitrogen and argon adsorption, 4) they calculated the pore size distribution (PSD) and pore wall thickness in their reference samples independently from different adsorption isotherms, and 5) they tested the consistency of the NLDFT model developed. This study provides an excellent framework in which to compare results from any other developed characterization method for these materials. Published works related to the experimental characterization of SBA-15 are those done by Ryoo et al. [47], and Kruk et al. [48-49]. Kruk et al.[48] synthesized SBA-15 following the procedure described by Zhao et al. [31], and then performed a systematic study of the structure of this material by means of XRD, termogravimetric analysis and nitrogen adsorption. The mesopore size distribution was calculated on the basis of adsorption branches of nitrogen isotherms using the BJH method with the corrected form of the Kelvin equation. They provided supported explanations for the existence of the complementary porosity arranged in a mesopore-micropore network as a result of the properties

of the triblock copolymer templates [48,49]. Additionally, they proposed an explanation of a plug formation mechanism that leads to the synthesis of PHTS adsorbents [49]. Ravikovitch and Neimark [13] were the first ones who characterized these materials within the DFT approach. They used nitrogen adsorption isotherms on SBA-15 materials prepared in different research groups, and applied a method for the characterization of SBA-15 based on non-local (NL) DFT, assuming cylindrical geometry. They just determined the size distribution of the main channels and the amount of the intrawall porosity, without characterizing the microporous region. The structural parameters obtained were in agreement with previous described geometrical considerations and XRD data. However, one of the shortcomings of their NLDFT model is that the calculated global adsorption isotherm exhibited pronounced layering (see figures 2 and 3 of reference [13]). They argued that this layering was an artifact caused by the use of the simplified, structureless pore wall model and/or approximations made in the DFT theory. Since in the present work we use MS instead of DFT to model the same materials, we will try to answer some of the questions raised by these authors.

The rest of the paper is organized as follows. In the next section we briefly present the modelling methodology used, including details on the application of the regularization procedure and the molecular simulations. The main results related to the structural characterization of the chosen materials, GCMC simulations and the robustness of the regularization procedure are presented and discussed in section three. Finally we summarize the main conclusions from this work in the last section.

2. METHODOLOGY

2.1. Molecular Model and Simulations

The adsorption behaviour in the selected materials is obtained by assuming the validity of the independent pore model [3]: the global adsorption behaviour of the material is due to the contribution of the individual pores with different diameters integrating the material, ignoring the effects derived from the connectivity among them. The same assumption is also known as the bundle of straight pores (BPS) model [20], equivalent to say that the material is represented by a bundle of pores each of which connects to the surface of the adsorbent, or, a connected network of pores in which the connectivity of the network is sufficiently good that the adsorptive species can pass throughout the network. Both models are equivalent regarding the global adsorption behaviour of the material. In most of the cases, they are a crude representation of adsorbent materials; however, this is the standard assumption made in most available methods to invert the global adsorption integral. The independent pore model

maybe too strong for tortuous, interconnected porous materials, but it should be accurate for MCM-41 materials, with unconnected pores [29]. It also seems a reasonable assumption for SBA-15 materials: they present two main pore ranges, one with a broad distribution of nano-micropores, and another one, more relevant for further applications, corresponding to a narrow mesopores distribution with a well defined pore size. Hence, we model the global adsorption of the materials in terms of several individual adsorption isotherms, obtained by GCMC simulations at different pressures and pore sizes.

The fluid-fluid interactions are modelled as single Lennard-Jones (LJ) spheres, with nitrogen parameters σ_{ff}= 0.3615 nm and ε_{ff}/k = 101.5 K, being k Boltzmann's constant. Those fluid-fluid parameters were chosen by Ravikovitch et al. [25] to fit bulk properties of the adsorbate, including liquid-gas surface tension and reference adsorption isotherms on nonporous substrates.

MCM-41 and SBA-15 are modelled as a collection of individual pores, assumed to be infinite cylinders with silica walls. The silica-gas interactions on such pores are modelled as the LJ interactions with an integrated smooth cylindrical layer of oxygen atoms. The structureless potential of the solid-fluid interaction used in this work is given by [50]

$$\phi_{wall}(r,R)=\pi^2\rho_s\varepsilon_{sf}\sigma_{sf}\left[\frac{63}{32}\left[\frac{r}{\sigma_{sf}}\left(2-\frac{r}{R}\right)\right]^{-10}F\left[-\frac{9}{2},-\frac{9}{2};1;\left(1-\frac{r}{R}\right)^2\right]-\right.$$
$$\left.-3\left[\frac{r}{\sigma_{sf}}\left(2-\frac{r}{R}\right)\right]^{-4}F\left[-\frac{3}{2},-\frac{3}{2};1;\left(1-\frac{r}{R}\right)^2\right]\right] \quad (1)$$

where the product $\rho_s\varepsilon_{sf}$ =22.5369 K Å^{-2}, being ρ_s=0.153Å^{-2} the effective surface number density of the oxygen atoms in the pore wall, ε_{sf} =147.3 K the LJ energy parameter between the solid and the fluid, and the combined molecular size solid-fluid parameter σ_{sf} = 0.317 nm. Those parameters were selected for comparative purposes with the previous work done in the system SBA-15/Nitrogen by Ravikovitch et al. [13], $F[\alpha,\beta,\gamma,\chi]$ are the hypergeometric functions [51]. The wall potential is calculated at a given distance r (in the radial direction) when the radius of the pore is R.

The individual adsorption isotherms are obtained by GCMC simulations. In GCMC, the temperature, T, the volume pore, V, and the chemical potential, μ, are kept fixed. The number of molecules is thus allowed to vary, and its average is the relevant quantity of interest. For convenience, to obtain the adsorption isotherm we ran simulations at different values of the activity [52], ξ, defined

as: $\xi = \left(\exp(\mu/kT)/\Lambda^3\right)$, where Λ is the De Broglie wavelength, which includes contributions from translational degrees of freedom, and μ, k, T were defined previously.

The usual magnitudes for representing adsorption data are the amount adsorbed in the pore versus the relative pressure p/p_0 in the bulk phase; here p_0 is the bulk saturation pressure. The activity is related to the pressure by $p/p_0 = \xi/\xi_0$, which implies that the bulk phase in thermodynamic equilibrium with the pore presents an ideal behaviour. We have checked that the corrections for the gas-phase nonideality were small, usually less than 10% in the value of p/p_0. The chosen state point for reduction of activities to pressures was the saturation point of pure nitrogen at 77 K, found to occur at ξ_0=0.0823 nm^{-3}. This result was calculated through a molecular-based equation of state, the soft-SAFT equation [53,54], using the nitrogen LJ parameters described above at needed conditions.

Most simulation runs required 2.5x10^8 configurations to reach the equilibrium. Additional 5x10^8 configurations were generated for average purposes. At some conditions longer runs were needed to accomplish the equilibrium conditions. Average properties were calculated over blocks with 5x10^5 configurations. The fluid-fluid potential was cut at r_c=5 σ_{ff} and no long range corrections were added. For a detailed discussion on the issue of the cutoff length and the addition of long range corrections in simulations of inhomogeneous fluids the reader is referred to reference [55].

To compare with experimental data, the excess pore fluid density was calculated as:

$$\langle \rho_{exc} \rangle = \frac{\langle N \rangle}{V} - \rho_{bulk} \tag{2}$$

where $\langle N \rangle$ is the mean number of particles inside the pore, ρ_{bulk} is the bulk density value at the same conditions, calculated from soft-SAFT [53,54], and V is the volume of the simulated pore.

2.2 Regularization procedure

The calculation of the PSD of porous materials from adsorption data has been addressed by several authors [8,13,20,21,26,48,49,56], using a variety of different available approaches. Among the different possibilities we have chosen to use Tikhonov's regularization method through a Singular Value Decomposition (SVD) as we consider it to be most adequate for PSD analysis purposes, for several reasons: 1) it is simple to implement, 2) it is very fast, as it

is a direct (as opposed to iterative) method, and 3) it is one of the best mathematically founded methods for that purpose. Hence we focus here on the mathematical details of the adaptable procedure of deconvolution over the adsorption integral equation followed in this work. The deconvolution procedure implies a grid size evaluation, i.e to select the number of pores and relative pressures to be included in the analysis, in addition to the adequate choice of the regularization parameter.

In order to obtain the PSD, *f(D)*, the adsorption integral equation should be inverted:

$$a_e(P) = \int_{D_{\min}}^{D_{\max}} A_s(P, D) f(D) dD \tag{3}$$

where $a_e(P)$ is the experimental adsorption isotherm at pressure P, $A_s(P, D)$ gives the single-pore adsorption isotherm for each pore-size D (in the range D_{min}-D_{max}), and it is the so-called kernel of the integral equation [57]. This problem is tantamount to that of solving a Fredholm integral equation of the first kind. As it is well known, this is an ill-posed problem, in the sense that the mapping $a_e \rightarrow f$, given by equation (3), is undefined because either the mapping is not continuous or the image f is not unique. From a practical point of view, the lack of continuity implies that f is highly sensitive to arbitrary small perturbations in the experimental data a_e. This poses a first problem of reproducibility of any solution to equation (3), and thus the problem, as stated before, has physically (and mathematically) no sense. Standard approaches [57] to this problem rely on solving the related problem of finding the solution f that minimizes the functional:

$$J[f] \equiv \left\| a_e(P) - \int_{D_{\min}}^{D_{\max}} A_s(P, D) f(D) dD \right\|^2 + \lambda^2 \left\| \int_{D_{\min}}^{D_{\max}} R(D', D) f(D) dD \right\|^2 \tag{4}$$

where $\| \ \|$ denotes an appropriate defined norm and λ is the so-called regularization parameter. The additional term renders the former problem into a well-defined one for each pair λ and $R(D', D)$, and corresponds to the Tikhonov´s regularization method.

In our case only a finite set of experimental data and simulations results are available. Thus, equation (3) becomes a system of linear equations $\mathbf{a}_e = \mathbf{A}_s\mathbf{x}$,

where $\mathbf{A}_s$ is a matrix of single-pore adsorption isotherms (m pressures × n pores). Here, $x_i = f(D_i)\Delta D_i$, where ΔD_i is the pore-size interval associated to the pore size D_i after discretizing equation (3). The corresponding regularized problem can be recast as:

$$\min_x \left\{ \left\| \mathbf{a}_e - \mathbf{A}_s \mathbf{x} \right\|_2^2 + \lambda^2 \left\| \mathbf{R}\mathbf{x} \right\|_2^2 \right\} \tag{5}$$

Although appropriate choices of the regularization term $\mathbf{R}$ may improve convergence to the unregularized solution [58], we will consider the simplest case of $\mathbf{R} = \mathbf{I}$ (the Identity matrix). The solution can then be obtained through a singular value decomposition (SVD) of the matrix $\mathbf{A}_s = \sum_{i=1}^{n} s_i \mathbf{u}_i \mathbf{v}_i^T$

$$\mathbf{x}_\lambda = \sum_i \frac{s_i^2}{s_i^2 + \lambda^2} \frac{\mathbf{u}_i^T \mathbf{a}_e}{s_i} \mathbf{v}_i \tag{6}$$

where s_i is the set of singular values of $\mathbf{A}_s$ that decay monotonously $s_1 \geq s_2 \geq \ldots \geq s_n \geq 0$ (assuming $m \geq n$), and $\mathbf{u}_i$ and $\mathbf{v}_i$ are the left and right singular vectors, respectively.

The SVD method requires the experimental data and the obtained kernel to fulfil a mutual suitability criterion given by the Discrete Picard Condition (DPC) [59]. This condition determines the convergence of f to the unregularized solution as well as the similarity between different solutions. The DPC requires that the Fourier coefficients $\left| \mathbf{u}_i^T \mathbf{a}_e \right|$ decay faster than s_i on average. The mathematical formulation is that the values r_i defined as:

$$r_i \equiv s_i^{-1} \left(\prod_{j=i-q}^{j=i+q} \left\| \mathbf{u}_i^T \mathbf{a}_e \right\| \right)^{1/(2q+1)} \tag{7}$$

should decay monotonically within some range of the high s_i. Here q is a small integer that determines the amount of averaging. Appropriate vales for q are 1, 2 or 3.

In addition, an adequate method for the selection of λ must be specified. There are different available methods which are not completely equivalent. The selection may depend on the specific problem. One of such method is the (generalized) discrepancy principle [57,58], which relies on having information of the experimental data error. The value of the regularization parameter is then

chosen such that the residual norm $\|\mathbf{a}_e - \mathbf{A}_s\mathbf{x}\|_2$ equals that error. Other methods rely on the particular mathematical properties of each selection scheme, e.g., the so-called *L-curve*. The latter is obtained by plotting the regularization term ||Rx|| versus the residual norm $\|\mathbf{a}_e - \mathbf{A}_s\mathbf{x}\|_2$ for different values of λ, thus obtaining a curve which mainly consists of two branches forming an "L". The corner of this curve provides a mathematically sound criterion for choosing the value of λ [58]. The basic criterion for any of these approaches is the condition that a good regularization parameter should yield a fair balance between the regularization term and the residual norm. Indeed, from the above discussion, we shall expect to have $0 < \|\mathbf{a}_e - \mathbf{A}_s\mathbf{x}\|_2$ within the experimental errors.

Although this formulation of the problem is mathematically sound, we still face many ambiguities from a physical point of view. First of all we have the very stringent condition *f(D)* to be a non-negative function (feasibility condition). Second, we aim at finding a systematic and robust procedure to determine a feasible solution. This means not only the obvious idea of robustness against errors in the experimental data and molecular simulations, which the regularization procedure already provides. We shall also require robustness against the very selection of the experimental data and the kernel to be used. In addition, this selection may affect the usual robustness against errors in the data. Thus, this raises the additional ambiguity of choosing a set of input data, as different sets show different robustness. In other words, different sets of experimental data and kernel should yield similar enough PSDs, and either a similar or an optimized robustness against errors in the input data.

Hence, a complete systematic procedure shall give a prescription for choosing a sound set of experimental data and the kernel to be used. Common mathematical procedures, as the one we use, are not guaranteed to neither satisfy nor completely answer these requirements. Therefore in order to obtain a reliable solution, further inspection of the given data is needed.

Guided by these ideas and considering the additional requirement of non-negativity of the solution $\mathbf{f}_\lambda^k > 0$, we have chosen λ as the smallest value for which this requirement is fulfilled λ_{feas}, i.e., the smallest λ for which a feasible solution is obtained. Note that since $\mathbf{v_i}$ changes more often sign as s_i decreases, f_0 becomes in general an unfeasible solution. We shall also require this value to lie close to the corner of the L-curve. The implicit assumption here is that the L-curve varies smoothly with the Lagrange parameter μ^2 corresponding to the additional feasibility constraint. Indeed the obtained values would lie close to the corner of the actual L-curve. Some preliminary results on this line were presented in reference [26], where some additional tests, besides the

mathematical requirements outlined above were pointed out. A throughout study on the applications of these requirements to two materials is presented here.

3. RESULTS AND DISCUSSION

Results on the systematic application of the methodology outlined in the previous section are presented and discussed here. In summary, in order to isolate the different effect mathematical or physical conditions may have in the obtained PSDs, we have developed and applied the following protocol:

(1) to chose the kernel size: number of pressure points and pore sizes to be simulated,
(2) to invert the integral equation with the Tikhonov regularization method through SVD,
(3) to check for the fulfilment of the DPC,
(4) to chose the regularization parameter best fulfilling the L-curve criteria and the physical condition that *f(D)* should be a non-negative function.

Once these four criteria are applied, we check the performance of the method for the global adsorption integral and the obtained PSD. Depending on the agreement with the experimental data the whole cycle is repeated, choosing a new kernel size and imposing the fulfilment of the mathematical requirements in the order just explained. We show here the effect of increasing the number of pores keeping constant the pressure points, as well as the importance of choosing the adequate range of pressures for the kernel. An additional test to check the robustness of the calculated PSD has been performed by adding random errors into the experimental data.

The experimental nitrogen adsorption isotherm of the selected MCM-41 material was taken from reference [11], while experimental data concerning the SBA-15 was obtained in our laboratory [29]. In order to perform a fair comparison between experimental and simulated results, it is important to note that the experimental adsorption isotherm represents the amount of fluid adsorbed per unit of mass of the solid, while the simulated adsorption isotherm represents the amount of adsorbed fluid per unit of void volume. These two concepts of volume are related by the true density and the porosity of the material. We have used the value of the true density as 2.2 g/cm^3 for pure silica. The porosity has been calculated by a trial and error procedure, checking that $\wp\int f(D)dD = 1$, where $\wp$ represents the porosity and *f(D)* is expressed in (length)$^{-1}$ units.

As a first step to invert Equation (3), one need to construct the kernel, that is, to select how many experimental pressures and individual pores isotherms will be considered. It is not clear, a priori, what the influence of these numbers will

be neither in the PSD obtained, nor in the global adsorption isotherm generated by fitting to the experimental one. Some of these issues were already investigated in [26]. We follow a similar procedure here.

In order to generate the kernel we have calculated a collection of individual adsorption isotherms, $A_s(P,D)$, using the GCMC method, in a diameter range of 0.75≤ D ≤14.0 nm, with 40 different pore diameters. This range covers from very narrow pores, well belonging to the micropores regime, to wide mesopores. For the case of the MCM-41 material 60 pressure points were selected for the MCM-41 from those reported in [11], as the starting point to construct the kernel. The pressure points for the SBA-15 kernel were chosen at the experimental relative pressure data.

With the calculated set of individual adsorption isotherms, and based on the analysis of the DPC, our next step is to determine how many pores are needed to fit a given set of experimental data by the regularization procedure. Figure 1 depicts the DPC, r_i, and its components (i.e. the Fourier coefficients $\left|\mathbf{u}_i^T\mathbf{a}_e\right|$ and the singular values s_i for different adsorption kernels $\mathbf{A}_s$ for the AM-5 material.

In the first five selected kernels for AM-5, the experimental number of relative pressures was fixed to m = 60 (interpolated along the experimental data of Neimark et al. [11]), while different sets of pore sizes were considered, n = 16, 22, 28, 30 and 34. In all cases the minimum and maximum pore diameter values were 0.75 nm and 5.40 nm, respectively. The selected pores included in the analysis were equally distributed between these two values. As it can be seen in Figure 1, all the studied cases fulfil the DPC. Also, from the r_i averages, there are not significant differences comparing q = 1 to q =3. Since, as mentioned in the prescribed protocol, this is the first criterion to be fulfilled, all the selected kernels can be used to check the fulfilment of the rest of the criteria.

The second test would be the application of the *L-curve* criterion to the kernels fulfilling DPC and the selection of the best λ_{feas}.

The values of λ_{feas} fluctuates with the value of n; for the particular cases studied here, with a fixed value of m = 60 (five first cases in Figure 1), the obtained values are 15.0, 18.6, 19.3, 16.5 and 23.2, respectively. The residual error fluctuates as follows $\left\|\mathbf{a}_e - \mathbf{A}_s\mathbf{x}\right\|_2$ = 6.636, 7.310, 5.118, 4.742 and 5.736. The modulus of $\mathbf{f}_{\lambda feas}$ decreases monotonously, $\left\|\mathbf{f}_{\lambda feas}\right\|$ = 0.762, 0.628, 0.529, 0.525 and 0.458.

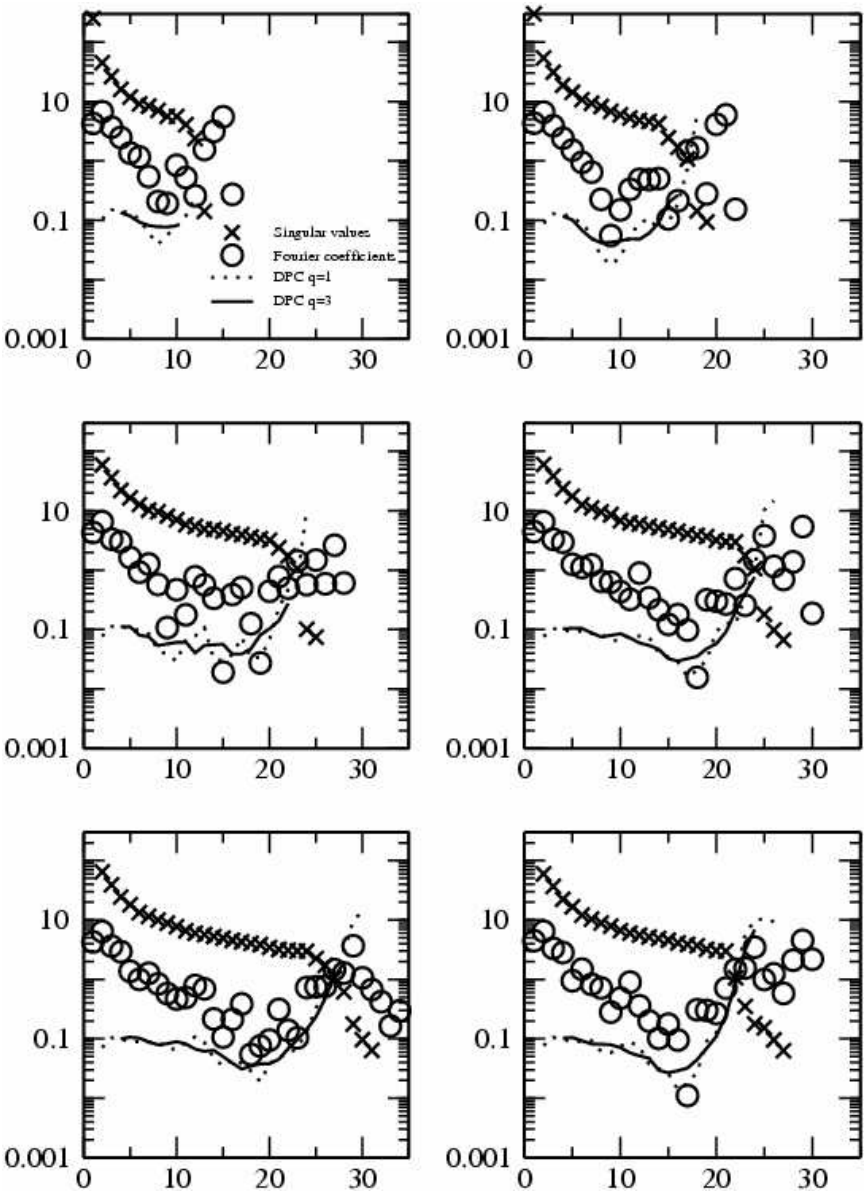

Fig. 1. The DPC condition for different kernel sizes for the AM5 material. Front left to right and top to bottom, in the five first cases the number of relative pressures is $m = 60$ and the number of pores are $n = 16$, 22, 28, 30 and 34. The right bottom corresponds to a kernel with $m = 54$ (see text for details). (O) absolute values of the Fourier coefficients, (X) singular values. The lines correspond to a plot of the averages r_i for $q = 1$ (dotted lines) and $q = 3$ (solid lines).

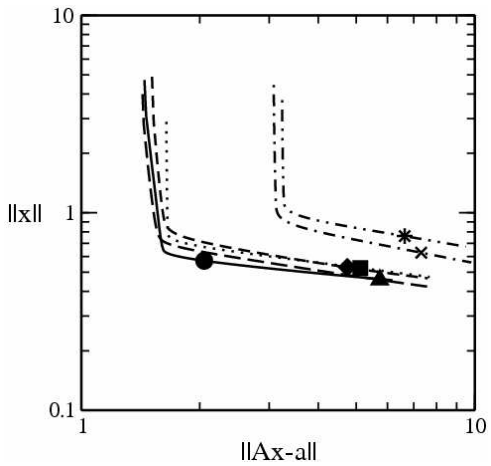

Fig. 2**.** The L-curve for m = 60 and n = 16, 22, 28, 30 and 34, with symbols corresponding to λ_{feas}, (✱),(x),(■),(◆) and (▲) respectively; m=54, n=30 is represented by a full line, λ_{feas} for the best solution is denoted by ●.

Once these criteria were applied to the first five kernels, we have checked the performance of the method for the global adsorption isotherm and the obtained PSD. We noticed that, although the overall agreement was good, the agreement with the experimental adsorption data could be improved in the region between 0.2 and 0.5 p/p_0. This is the reason why we have included a new kernel in the analysis with m = 54, in which the pressure range near the inflexion point in the adsorption curve is better refined. The selected number of pores for the kernel was n = 30, since no improvement was found when increasing the number of pores from 30 to 34 (see Fig. 1). Following the prescribed protocol for any kernel under study, we have applied the same procedure as for the other five kernels; the fulfilment of DPC criterion for this kernel was shown in Figure 1 and the L-curve criterion in Figure 2. The obtained values for this case were: λ_{feas}=6.8, $\left\|\mathbf{a}_e - \mathbf{A}_s\mathbf{x}\right\|_2$=2.05 and $\left\|\mathbf{f}_{\lambda feas}\right\|$= 0.572, showing the smallest value of λ_{feas} about the six one investigated and the smallest residual error.

Although, in principle, we have several feasible solutions and a well sounded solution (54x30), it is well known that there are associated errors to the experimental data; it should be of relevance to know the effect that these errors would have in the obtained PSD, showing the robustness of the procedure. Hence, we have applied a third criterion, over the six studied kernels, based on the effect of Gaussian random errors in the (experimental) data, $\mathbf{a}_e^* \rightarrow \mathbf{a}_e + \mathbf{e}$. We have generated the error, **e,** after choosing its variance. This is done through

a scaling factor *r* such that $\mathbf{a}_e^* = \mathbf{a}_e(1 + rz)$, where z is a Gaussian random number. The value of *r* is chosen such that on average at least 99% of the perturbed values correspond to relative errors not greater than the experimental ones. In the particular cases we are considering here we have chosen *r* = 0.02, and the average values over 50 realizations for the six kernels. The corresponding average values after perturbation are λ_{feas} = 14.4, 18.9, 18.4, 19.1, 22.7 and 22.1, $\left\|\mathbf{a}_e^* - \mathbf{A}_s\mathbf{x}^*\right\|_2$ = 7.171, 7.905, 5.859, 6.362, 6.683 and 5.274 (following the same sequence as Figure 1). The relative PSD variations on average are, respectively, $\left\|\mathbf{f}_{\lambda feas} - \mathbf{f}_{\lambda feas}^*\right\| / \left\|\mathbf{f}_{\lambda feas}\right\|$ = 0.049, 0.055, 0.048, 0.049, 0.049 and 0.030. Results are summarized in Figure 3. As it can be observed in the figure, the 54x30 kernel is the most robust among the six studied here.

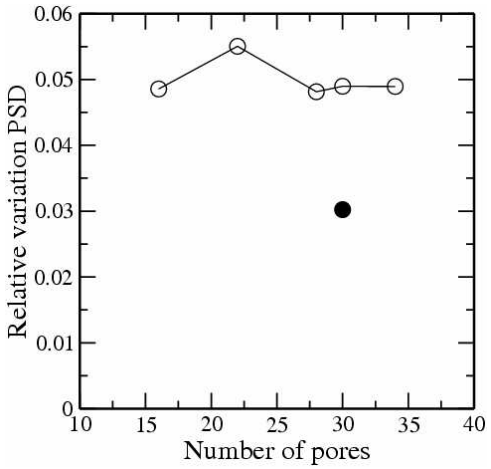

Fig. 3. Graphical representation of the average relative error (over 50 perturbations) of the obtained PSD *f(D)* versus the index *n*. Symbols: (○) different kernels fulfilling DPC (see Fig. 1) with *m* = 60, (●) the single value for *m* = 54. The solid line is a guide to the eyes.

Figure 4 shows the comparison between the experimental and the calculated adsorption isotherm with two selected kernels. Note that although both of them give an overall excellent representation of the adsorption behaviour, the 54x30 kernel provides a better description of the abrupt changes in the curve.

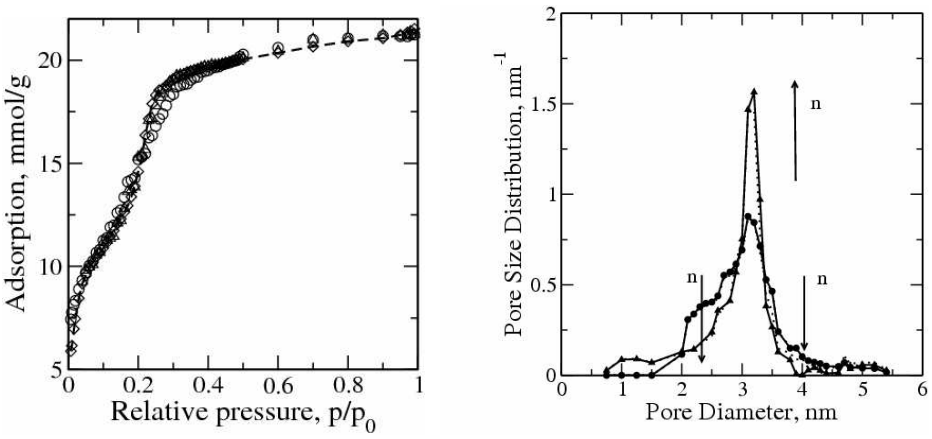

Fig. 4. Calculated results for two of the best kernels presented in Figures 1-3. (a) Experimental (◇) and simulated adsorption isotherms; (b) PSD obtained with the two selected kernels for AM5, (●) 60x34 and (▲) 54x30 kernels, respectively. In (b) solid lines correspond to results for unperturbed data and dotted lines are a representative example of their corresponding perturbed cases.

The robustness of the 54x30 kernel is also observed in Figure 4(b), where the PSD for 60x34 and 54x30 are plotted with their corresponding perturbation $\|\mathbf{e}\|$. The dotted lines correspond to a particular case where a perturbation to $\|\mathbf{a}\|$ has been added, while the continuous lines correspond to the unperturbed cases. Note that although the shape of the PSD function is not exactly the same, being less defined in the 60x34 case, both kernels provide exactly the same value for the peak of the distribution, both of them have captured the relevant pore size of the material.

Finally, we compare in Figure 5 results obtained with our approach (for the case of 54x30) with previous published results obtained for the same material from Neimark et al. [11]. The agreement obtained is excellent. Using the described methodology the mean pore for AM-5 is found around 3.2 nm, in excellent agreement with the value reported in [11]. Note that there are two important differences in the way the PSD was obtained here and in [11]. Neimark et al. used DFT instead of GCMC to generate the individual adsorption isotherms and they inverted the adsorption integral following a different mathematical procedure.

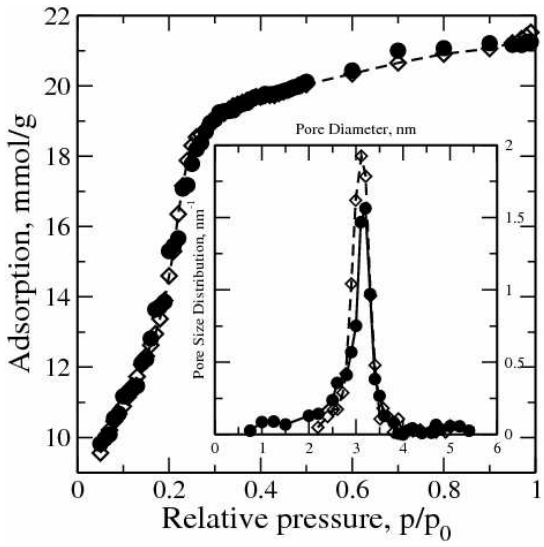

Fig. 5. The simulated adsorption isotherm for AM-5 obtained from the 54x30 kernel. Inset, the calculated PSD compared with the one proposed by Neimark [11] (●) this work; (◇) Neimark et al.

From the previous detailed discussion on the different aspects to be considered when calculating PSD we can conclude that the methodology used is accurate to characterize the adsorption in MCM-41 materials. This proves that the mathematical procedure and the molecular model are accurate for obtaining sounded PSDs for materials with unconnected pores; the next step is to use the same methodology to characterize porous materials in which pores have a well-defined geometry but there are some connections among them. As stated in the introduction, we have chosen the SBA-15 for its particular structure as well as for its potential applications in several fields of interest.

The characterization of the SBA-15 material has been performed following a similar procedure to the MCM-41 material described above, including the assumption of the independent pore model for the inversion of the integral equation. Hence, some of the details described will be omitted here. Following the same protocol, the first step is to choose a kernel and to study the fulfilment of the different mathematical and physical criteria.

In the selected cases for the SBA-15 material the experimental number of relative pressures was fixed to m = 38, from the experimental minimum relative pressure value of 9.86×10^{-3} till a relative pressure of 0.93. Four different sets of pore sizes were evaluated, two with less pores than the number of pressure points, one with an equal number, and one with a greater number of pores

(n = 16, 20, 38, 40 respectively). In all cases the minimum and maximum pore diameter values were 0.75 nm and 14.0 nm, respectively. The selected pores included in the analysis were equally distributed between these two values. Contrary to the MCM-41 material, no all selected kernels fulfilled the DPC condition in this case, since the case n = 16 (not shown here) presented a monotonous increasing trend (opposite to what it should be). As mentioned, this is the first criteria to be fulfilled. As previous results [29] showed, the small size of the kernels used seems to enhance fluctuations in the Fourier coefficient. Thus, the other three cases have a similar fulfilment of the DPC, and should not be discarded with just this criterion.

The second test to be performed to the kernels fulfilling DPC would be the application of the L-curve criteria. Results are shown in Figure 6 (a). We have observed that the values of λ_{feas} tend to increase monotonously as n increases, the values of λ_{feas} are 2.3, 4.4 and 4.7, respectively. The residual error fluctuates as follows $\left\|\mathbf{a}_e - \mathbf{A}_s\mathbf{x}\right\|_2$ = 2.02, 0.67 and 0.71. The modulus of $\mathbf{f}_{\lambda feas}$ decreases monotonously, $\left\|\mathbf{f}_{\lambda feas}\right\|$ =0.746, 0.524, 0.519. Hence, according to the defined criteria, three of the studied kernels (38x20, 38x38 and 38x40) fulfil DPC, while the 38x38 and 38x40 give similar L-curve and residual error. Hence, one would be able to choose between these two. The average relative error of the PSDs obtained by these three kernels is presented in Figure 6 (b). As for the AM-5 case, we have chosen r = 0.02 for the scaling factor to be used in generating the Gaussian random errors. The average values over 50 realizations for the three kernels are $\left\|\mathbf{e}\right\|/\left\|\mathbf{a}_e\right\|$=0.0176, 0.0183 and 0.018, respectively.

Adsorption results and PSD's for the case of SBA-15 and the kernels corresponding to Figure 6 are summarized in Figure 7. The corresponding average values after perturbation are λ_{feas} = 6.90, 10.73 and 13.03 $\left\|\mathbf{a}_e^* - \mathbf{A}_s\mathbf{x}^*\right\|_2$ = 3.21, 2.61 and 2.98. The relative PSD variations on average are, respectively, $\left\|\mathbf{f}_{\lambda feas} - \mathbf{f}_{\lambda feas}^*\right\|/\left\|\mathbf{f}_{\lambda feas}\right\|$ = 0.228, 0.260 and 0.258. The robustness of the PSDs can be observed in Figure 7 (b), where the PSD is plotted for the above-mentioned values of n and their corresponding perturbation $\left\|\mathbf{e}\right\|$. The dotted lines correspond to the case where a perturbation to $\left\|\mathbf{a}\right\|$ has been added, while the continuous lines correspond to the unperturbed cases. It is also observed in Figure 7 that the "noise" obtained in the PSD for wider pores decreases as n increases.

Although the previous 38x20, 38x38 and 38x40 kernels had the prescribed requirements, we have performed a further study with an additional kernel of 38x31.

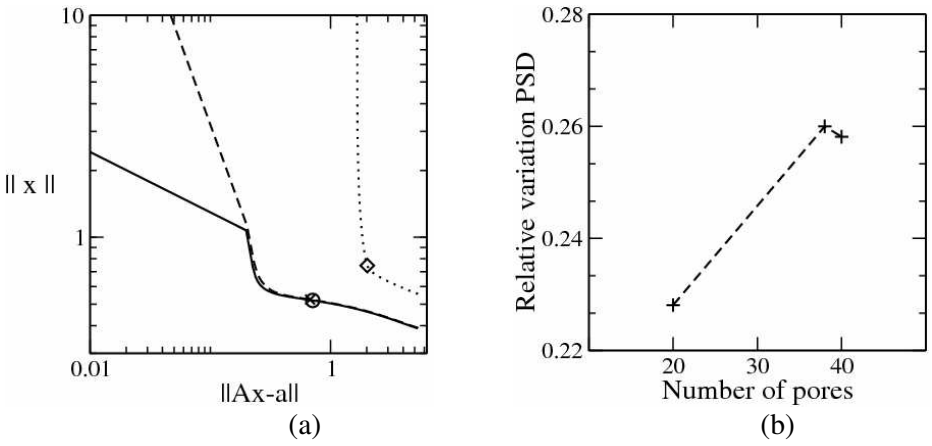

Fig. 6. Mathematical check of the conditions to be fulfilled by the different kernels describing the adsorption in SBA-15 (a) the L-curve for n = 20, 38 and 40, symbols corresponding to λ_{feas}, ◇ (dotted line), x (dashed line), and O (solid line), respectively. (b) the average relative error (over 50 perturbations) of the obtained PSD $f(D)$ versus n.

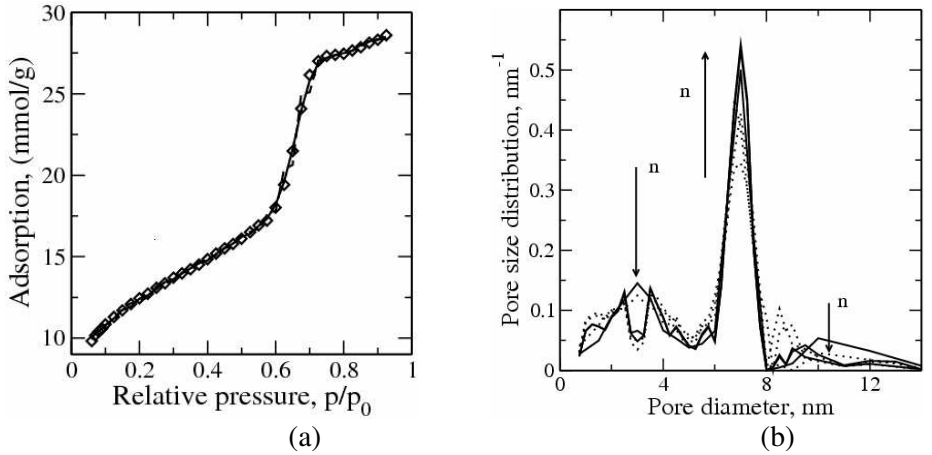

Fig. 7. Calculated results for SBA-15 from the three kernels shown in Figure 6 (a) Experimental (◇) and simulated adsorption isotherms. Symbols as in Figure 5; (b) PSD obtained with the three selected kernels. Continuous lines correspond to results for unperturbed data and dotted lines are a representative example of their corresponding perturbed cases.

The particular number of pores was chosen searching for the minimum number of pores that would provide a good description of the adsorption isotherm, including the capillary condensation pressure range. Since the analysis with 38

and 40 pores gave similar results, 31 pores could be enough, in principle, to capture the capillary step trend. A similar study to the previous four kernels was performed (DPC, L-criteria, residual error values and random errors into the experimental data). This turned out to be the best among the five selected in the present study. Results for the global adsorption isotherm as compared to the experimental data for SBA-15 with this selected kernel are shown in Figure 8, where we also show the corresponding PSD. The predicted adsorption behaviour is found in excellent agreement with the experimental results. The calculated GCMC PSD presents a sound shape for these materials, with a narrow distribution of mesoporous around 70.0Å, shifted in 16.7Å to the right of the BJH average prediction. The left extreme of the PSD is attributed to presence of the nano and microporous equal or smaller than 30 Å [48].

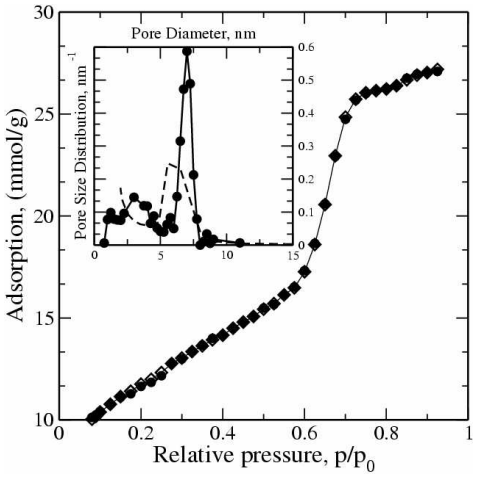

Fig. 8. The adsorption isotherm and PSD of SBA-15 obtained from kernel 38x31. The inset shows the comparison with the PSD obtained from the BJH as obtained from the software of ASAP 2010 V4.00 (Micromeritics Instrument Corporation).

Table 1 summarizes the best values obtained for the two selected materials, including the pore range, kernel size, λ_{feas}, residual error and relative PSD variation.

Tab. 1. Summary of Relevant Results for the Studied Materials

material	pore range, nm	kernel size	λ_{feas} [a]	$\|a-Ax\|$ [a,b]	RPSDV [b,c]
AM-5	0.75 – 5.4	54 x 30	6.8	2.05	0.03
SBA-15	0.75 – 14.0	38 x 31	10.3	2.45	0.11

[a] Corresponds to an average over 50 realizations of the perturbation.
[b] Dimensions of $\|Ax-a\|$ cm^3 STP/g, [c] The relative PSD variation.

As a final comment, we should point out that excellent agreement for the global adsorption isotherm has been obtained for both materials following the simulation-regularization procedure. Since the model used here for SBA-15 and that of Ravikovitch and Neimark [13] is the same, we can argue that the pronounced layering on the calculated isotherm obtained by their NLDFT is just an intrinsic shortcoming of the approximations made in the theory they used, and it is not due to the smoothness of the walls. The simulation technique seems to be more accurate for this type of studies, in spite of the extra computing time.

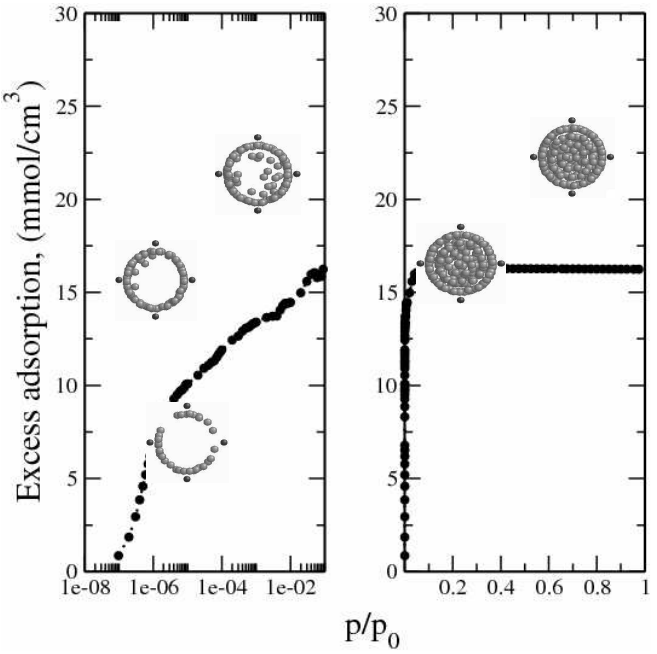

Fig. 9. Individual nitrogen adsorption isotherm at 77K for silica-based materials obtained by GCMC. D=3.0 nm. The figure on the left is a close-up of the low pressure region, while the figure on the right shows the complete adsorption isotherm. The inner pictures resemble the information we may lose about the filling process if the isotherm does not explore the low pressures region.

An additional advantage of using simulations is that the location of the molecules inside the pore is precisely known at any conditions. This can help to elucidate the adequate conditions in which to run the experiments. For instance, the microporous range of the material could be better tracked if high-resolution adsorption isotherms are provided. This can be inferred just by observing the equilibrium configurations of selected pore at selected pressures, as shown in Figure 9. In addition to the global adsorption isotherm, this figure presents snapshots of the adsorption process taking place inside the individual pore of the

diameter D = 3.0 nm, for selected relative pressures (see Fig. 9). The lowest relative pressure in the experiments was measured at 9.86×10^{-3}; note that for this pore the monolayer is already filled at this pressure. Since this information is lost, this will clearly affect the PSD and surface area calculations.

4. SUMMARY AND CONCLUSIONS

We have presented a protocol which can be applied in combination with experimental adsorption data in order to obtain robust and reliable PSDs of different materials. The methodology is based on the generation of individual adsorption isotherms from GCMC, with an adequate mathematical procedure, based on regularization methods, to invert the adsorption isotherm. Some additional physical and mathematical requirements are also imposed, all of them leading to the most robust and sounded solution.

We have checked the validity of this methodology for two selected materials, MCM-41 and SBA-15. The a priori selection of these materials comes from their particular structure and for their potential applications in several fields. They both present well-defined pore geometry (cylindrical). In addition, MCM-41 presents a unimodal and narrow PSD, attainable from other experimental techniques and geometrical considerations. SBA-15 is a material with a PSD presenting two distinct ranges (micro and mesoporous).

In particular, PSDs were obtained by a deconvolution procedure in which a grid size evaluation and several choices of parameters were studied. The addition of perturbations over the experimental adsorption data was used to check the robustness of the obtained PSD. The excellent agreement found between the calculated and the experimental adsorption isotherms corroborates the validity of the independent pore model for these materials, as well as the method used to generate the kernel. The PSDs provided by this procedure show pore sizes in accordance to published values obtained from alternative experimental procedures and geometrical considerations, reassuring the validity of our methodology. A comparison with BJH calculations shows, as was expected, that the latest underestimates the pore sizes present in the material. The excellent agreement found and the robustness of the PSDs versus experimental errors prove by themselves the success of the methodology for these types of materials.

Finally, GCMC has proved to be a straightforward method, affordable nowadays, to generate the individual adsorption isotherms, more accurate that DFT approaches. It also provides additional insights into the best conditions to perform the experiments. A main advantage of using molecular simulations is that this methodology can be easily extended to investigate the behaviour of other materials and/or the adsorption of more complex fluids inside the characterized materials. GCMC can be an excellent tool to investigate the

optimum conditions for specific applications of these materials, in a predictive manner.

Acknowledgments. We are grateful to our experimental collaborator, F. Medina, who strongly motivated this work and who has supported us since the beginning of the project. We are also thankful to M. Jaroniec for suggesting the selection of the MCM-41 material. This research has been possible thanks to the financial support received from the Spanish Government, under projects PPQ2001-0671 and CTQ2004-05985-C02-01.

REFERENCES

[1] S. J. Gregg and K. S. W. Sing, *Adsorption, Surface Area and Porosity*, Academic Press: New York. (1982).
[2] R. Evans and P. Tarazona, *Phys. Rev. Lett*. 52, 557(1984).
[3] N. A. Seaton, J. P. R. B. Walton, Quirke N. *Carbon* 27, 853(1989).
[4] P. N. Aukett, N. Quirke, S. Riddiford, S. R. Tennison, *Carbon* 30, 913 (1992).
[5] C. Lastoskie, K. E. Gubbins, N. Quirke, *J. Phys. Chem*. 97, 4586 (1993).
[6] N. Quirke, S. R. N. Tennison, *Carbon* 34, 1281 (1996).
[7] K. A. Sosin, D. F. Quinn, *J. Porous Mater*. 1, 111(1995).
[8] S. Figueroa-Gerstenmaier, J. Bonet Avalos, L. D. Gelb, K. E. Gubbins, L. F. Vega, *Langmuir* 19, 8592 (2003).
[9] S. Figueroa-Gerstenmaier *Development and Application of Molecular Modeling Techniques for the Characterization of Porous Materials*, PhD Dissertation, Universitat Rovira i Virgili, Tarragona (2002).
[10] P. I. Ravikovitch, S. C. O. Domhnaill, A. V. Neimark, F. Schueth, K. K. Unger, *Langmuir* 11, 4765 (1995).
[11] A. V. Neimark, P. I. Ravikovitch, M. Grün, F. Schüth, K. K. Unger, *J. Colloid Interface Sci.* 207, 159 (1998).
[12] K. Schumacher, P. I. Ravikovitch, A. Du Chesne, A. V. Neimark, K. K. Unger, *Langmuir* 16, 4648 (2000).
[13] P. I. Ravikovitch, A. V. Neimark, *J. Phys. Chem. B.* 105, 6817 (2001).
[14] D. J. Adams, *Mol. Phys.* 28, 1241 (1974).
[15] K. A. Sosin, D. F. Quinn, J. A. F. MacDonald, *Carbon* 34(11), 1335 (1996).
[16] V. Y. Gusev, J. A. O'Brien, *Langmuir* 13, 2822 (1997).
[17] S. Saimos, A. K. Stubos, N. K. Kanellopoulos, R. F. Cracknell, G. K. Papadopoulos, D. Nicholson, *Langmuir* 13, 295 (1997).
[18] B. McEnaney, T. J. Mays, X. Chen, *Fuel* 77(6), 557 (1998).
[19] G. M. Davies, N. A. Seaton, *Carbon* 36, 1473 (1998).
[20] G. M. Davies, N. A. Seaton, *Langmuir* 15, 6263 (1999).
[21] G. M. Davies, N. A. Seaton, V. S. Vassiliadis, *Langmuir* 15, 8235 (1999).
[22] K. Koch, M. v. Szombathely, N. Neugebauer, P. Brauer, In: *Fundamentals of Adsorption*; LeVan, M. D., Ed.; Kluwer: Boston, 1996; p. 921.
[23] J. P. Oliver, W. B. Conklin, M. v. Szombathely, *Characterization of Porous Solids (COPS-III)*. Proceedings of the IUPAC Symposium; Rodriguez-Reinoso F.; Rouquerol J.; Sing K. S. W.; Unger K. K., Eds.; Elsevier: Amsterdam, (1994); p. 81.

[24] C. A. Jessop, S. M. Riddiford, N. A. Seaton, J. P. R. B. Walton, N. Quirke, in *Characterization of Porous Solids (COPS-III).* Proceedings of the IUPAC Symposium; Rodriguez-Reinoso F.; Rouquerol, J.; Sing K. S. W.; Unger K. K., Eds.; Elsevier: Amsterdam, (1994); p. 123.
[25] P. I. Ravikovitch, A. Vishnyakov, A. V. Neimark, *Physical Review E*. 64, 011602 (2001).
[26] C. Herdes, M. A. Santos, S. Abelló, F. Medina, L. F. Vega, *Applied Surf. Sci*. (2005) *in press*
[27] F. J. Blas, L. F. Vega, K. E. Gubbins, *Fluid Phase Equil.* 150-151, 117 (1998).
[28] S. Figueroa-Gerstenmaier, F. J. Blas, J. Bonet Avalos, L. F. Vega, *J. Chem. Phys*. 118, 830 (2003).
[29] C. Herdes, M. A. Santos, F. Medina, L. F. Vega, *Langmuir* (2005) submitted.
[30] C. T. Kresge, M. E. Leonowicz, W. J. Roth, J. C. Vartuli, J. S. Beck, *Nature* 359, 710 (1992).
[31] T. F. Degnan, I. D. Johnson, K. M. Keville, U. S. Patent No. 5,156,828 (1992).
[32] J. S. Beck, J. C. Vartuli, W. J. Roth, M. E. Leonowicz, C. T. Kresge, K. D. Schmitt, C. T.-W. Chu, D. H. Olson, E. W. Sheppard, S. B. McCullen, J. B. Higgins, J. L. Schlenker, *J. Am. Chem. Soc*. 114, 10834 (1992).
[33] J. C. Vartuli, C. T. Kresge, M. E. Leonowicz, A. S. Chu, S. B. McCullen, I. D. Johnson, E. W. Sheppard, *Chem. Mater*. 6, 2070 (1994).
[34] J. C. Vartuli, K. D. Schmitt, C. T. Kresge, W. J. Roth, M. E. Leonowicz, S. B. McCullen, S. D. Hellring, J. S. Beck, J. L. Schlenker, D. H. Olson, E. W. Sheppard, *Chem. Mater*. 6, 2317 (1994).
[35] A. Monnier, F. Schuth, Q. Huo, D. Kumar, D. Margolese, R. S. Maxwell, G. D. Stucky, M. Krishnamurty, P. Petroff, A. Firouzi, M. Janicke, B. F. Chmelka, *Science* 261, 1299 (1993).
[36] Q. Huo, D. I. Margolese, G. D. Stucky, *Chem. Mater*. 8, 1147 (1996).
[37] W. Kolodziejski, A. Corma, M.-T. Navarro, J. Pérez-Pariente, *Solid State Nucl. Magn. Reson*. 2, 253 (1993).
[38] D. Zhao, Q. Huo, J. Feng, B. F. Chmelka, G. D. Stucky, *J. Am. Chem. Soc*. 120, 6024 (1998).
[39] P. Van Der Voort, P. I. Ravikovitch, K. P. De Jong, M. Benjelloun, E. Van Bavel, A. H. Janssen, A. V. Neimark, B. M. Weckhuysen, E. F. Vansant, *J. Phys. Chem B*. 106, 5873 (2002).
[40] M. Cheng, Z. Wang, K. Sakurai, F. Kumata, T. Saito, T. Komatsu, T. Yashima, *Chem Lett.* 131 (1999).
[41] Z. Luan, M. Hartmann, D. Zhao, W. Zhou, L. Kevan, *Chem. Mater*. 11, 1621 (1999).
[42] Y. Yue, A. Gedeon, J.-L. Bonardet, N. Melosh, J.–B. D'Espinose, J. Fraissard, *Chem. Commun.* 1967 (1999).
[43] Z. Luan, E. M. Maes, P. A. W.Van Der Heide, D. Zhao, R. S. Czernuszewicz, L. Kevan, *Chem. Mater*. 11, 3680 (1999).
[44] S. J. Bae, S. –W.Kim, T. Hyeon, B. M. Kim, *Chem. Commun*. 31 (1999).
[45] Y. –J.Han, G. D.Stucky, A.Butler, *J. Am. Chem. Soc*. 121, 9897 (1999).
[46] P. Yang, G. Wirnsberger, H. C. Huang, S. R. Cordero, M. D. McGehee, B. Scott, T. Deng, G. M. Whitesides, B. F. Chmelka, S. K. Buratto, G. D. Stucky, *Science* 287, 465 (2000).
[47] Ryoo R, C. H. Ko, M. Kruk, V. Antochshuk, M. Jaroniec, *J. Phys. Chem. B* 104, 11465 (2000).
[48] M. Kruk, M. Jaroniec, C. H. Ko, R. Ryoo, *Chem Mater*. 12, 1961 (2000).
[49] M. Kruk, M. Jaroniec, S. H. Joo, R. Ryoo, *J. Phys. Chem. B* 107, 2205 (2003).
[50] G. J. Tjatjopoulos, D. L. Feke, J. A. Mann Jr., *J. Phys. Chem.* 92, 4006 (1988).
[51] W. A. Press, S. A. Teukolsky, W. T. Vetterling, B. P. Flanery, *Numerical Recipes in Fortran*, 2nd edition, Cambridge University Press, U.S.A. (1992), Chap 6, p. 263.

[52] M. P. Allen, D. J. Tildesley, *The Computer Simulation of Liquids*, Clarendon Press, Oxford. (1987).
[53] F. J. Blas, L. F. Vega, *Mol. Phys.* 92, 135 (1997).
[54] J. C. Pàmies, L. F. Vega, *Ind. Eng. Chem. Res*. 40, 2532 (2001).
[55] D. Duque, L. F. Vega, *J. Chem. Phys.* 121(17), 8611 (2004).
[56] P. Kowalczyk, P. A. Gauden, A. P. Terzyk, D. D. Do, G. Rychlicki, Annales Universitatis Mariae Curie-Sklodowska, Sectio AA, vol. LVII, 2, 46 (2002).
[57] C. W. Groetsch, *The Theory of Tikhonov Regularization for Fredholm Equations of the First Kind*, Pitman Publishing, (1984).
[58] P. C. Hansen, *SIAM Review* 24(4) 561 (1992).
[59] P. C. Hansen, *BIT* 30, 4, 658 (1990).
[60] J. H. de Boer, *The Structure and Properties of Porous Materials*, Butterworth, London (1958).
[61] L. H. Cohan, *J. Am. Chem. Soc.* 60, 433 (1938).
[62] M. B. Coelingh, *PhD Thesis*, Utrecht (1938).

CURRICULLUM VITAE

Lourdes F. Vega was born in Villanueva del Fresno (Badajoz), Spain in 1965. She graduated from the Faculty of Physics at University of Sevilla in 1988. She spent two years (1990-1992) as a Visiting Scholar at the University of Southern California, LA, USA, under the supervision of Prof. Katherine Shing, where she worked on the development of molecular simulation algorithms for phase equilibria calculations. She received Ph. D. degree in Physics (Cum Laude per Unanimity) from the University of Sevilla in 1992. After graduation she joined the groups of Profs. Gubbins and Panagiotopoulos at Cornell University as a Postdoctoral Researcher. In 1995 she became professor in Chemical Engineering at the Rovira i Virgili University (Tarragona), Spain. As a professor she had managed and designed several different courses and study programs, at the undergraduate and graduate level, distributed among the University of Sevilla, Cornell University, Rovira i Virgili University and the Autonomous University of Barcelona. In 2003 she became a Senior Scientist at the Spanish Council for Research (CSIC). She is the author of more than 50 scientific articles in prestigious international journals and has defended over 100 presentations in international conferences. She is the leader of Molecular Simulation Group at "Institut de Ciència de Materials de Barcelona" (ICMAB--CSIC). The main goal of the group is the application of the Molecular Modelling techniques (theory and simulation) to industrial relevant problems. The group is focused on two main research lines: thermodynamic and transport properties of complex fluids, including polymers, surfactants, micelles and aqueous solutions and modelling, characterization, design and application of selected materials for specific applications.